arXiv:1212.3661v3 [cond-mat.mtrl-sci] 24 Jan 2013

Spin-dependent inter- and intra-valley electron-phonon scattering in germanium

Z. Liu,[1] M. O. Nestoklon,[2] J. L. Cheng,[3] E. L. Ivchenko,[2,*] and M. W. Wu[1,†]
[1]Hefei National Laboratory for Physical Sciences at Microscale and Department of Physics,
University of Science and Technology of China, Hefei, Anhui, 230026, China
[2]A. F. Ioffe Physico-Technical Institute, Russian Academy of Sciences, St. Petersburg 194021, Russia
[3]Department of Physics and Institute for Optical Sciences, University of Toronto,
60 St. George Street. Toronto, Ontario, Canada M5S 1A7

(Dated: January 25, 2013)

We investigate the spin-dependent electron-phonon scatterings of the L and Γ valleys and the band structure near the conduction band minima in germanium. We first construct a 16×16 $\boldsymbol{k} \cdot \boldsymbol{p}$ Hamiltonian in the vicinity of the L point in germanium, which ensures the correctness of the band structure of the lowest three conduction bands and highest two valence bands. This Hamiltonian facilitates the analysis of the spin-related properties of the conduction electrons. We then demonstrate the phonon-induced electron scatterings of the L and Γ valleys, i.e., the intra-Γ/L valley, inter–Γ-L valley and inter–L-L valley scatterings in germanium. The selection rules and complete scattering matrices for these scatterings are calculated, where the scattering matrices for the intra-Γ valley scattering, inter–Γ-L valley scattering and the optical-phonon and the separated transverse-acoustic- and longitudinal-acoustic-phonon contributions to the intra-Γ valley scattering have not been reported in the literature. The coefficients in these scattering matrices are obtained via the pseudo-potential calculation, which also verifies our selection rules and wave-vector dependence. We further discuss the Elliott-Yafet mechanisms in these electron-phonon scatterings with the $\boldsymbol{k}\cdot\boldsymbol{p}$ eigenstates at the L and Γ valleys. Our investigation of these electron-phonon scatterings are essential for the study of the optical orientation of spin and hot-electron relaxation in germanium.

PACS numbers: 61.72.uf, 71.70.Ej, 72.10.Di, 78.60.Fi

I. INTRODUCTION

The group IV materials are attractive and promising candidates for the achievement of spintronic devices.[1–20] The Dyakonov-Perel mechanism is absent in these materials due to the centrosymmetry and the hyperfine interaction can be suppressed by isotopic purification, which ensures a relative long spin-decoherence time.[1,3,10,12,21–25] Also, the silicon-based microfabrication technology is well-developed and extensively used.[3] Germanium (Ge), as a group IV element adjacent to silicon, shares the good spin-decoherent property and is fully compatible with the existing mature nanoelectronic technology in silicon (Si).[2,10,12,16] Particularly, in contrast to Si, Ge shows obvious electro-optic effect as its direct gap (at the Γ point) is close to the indirect gap (at the L point) and lies in the infrared range.[11–19,26,27] Thus the optical orientation of carriers, which is free from the interfacial effect and the external electric and magnetic fields, can be carried out effectively in Ge-based devices.[11,12,16,28] Moreover, compared with Si, the longer spin-diffusion length stemming from the larger carrier mobility is helpful to the spin injection and the relative strong spin-orbit coupling benefits the manipulation of spin.[10,12,14,16,17]

In recent years, Ge attracts a renewed interest both experimentally and theoretically. In the experimental side, Loren *et al.*[10,12] and Pezzoli *et al.*[16] demonstrated the optical injection and detection of polarized electrons and holes in bulk Ge and Ge-based quantum wells, where electrons are pumped optically in the Γ valley and quickly scattered to the indirect valleys. In the theoretical side, a progress was made in investigations of the conduction band structure and spin-dependent electron-phonon scattering.[11,13,15,18] A compact 10×10 $\boldsymbol{k} \cdot \boldsymbol{p}$ Hamiltonian was constructed around the L point via the method of invariant.[18,29–31] Moreover, Tang *et al.*[15] derived the selection rules for intra- and inter-L valley electron-phonon scattering, and calculated the average absolute values of corresponding scattering elements within the tight-binding model. Later Li *et al.*[18] demonstrated the scattering matrices for the inter-L valley scattering and acoustic (AC) contribution to the intra-L valley scattering by using the pseudo-potential method, where the approximated wave-vector dependence of the intra-L valley scattering is derived with the combination of $\boldsymbol{k}\cdot\boldsymbol{p}$, pseudo-potential and group theories.[32] Very recently Li *et al.*[19] also reported the selection rules of the intra–Γ-L valley electron-phonon scattering in the calculation of phonon-assisted optical transitions in Ge. However, to our knowledge, the complete scattering matrices of several important channels of the electron-phonon scattering have not been discussed yet, such as the intra-Γ valley scattering, the optical-phonon (OP) contribution to the intra-L scattering as well as the inter–Γ-L valley scattering. As shown in previous works, these scatterings are fundamental to understand the spin dynamics in the optical orientation of electron spin in Ge.[10–12,16,19]

In this work, we readdress the band structure of Ge near the conduction band minima and study the phonon-induced electron scatterings in the L and Γ valleys. We first derive a spin-dependent 16×16 $\boldsymbol{k}\cdot\boldsymbol{p}$ Hamiltonian in the vicinity of the L point in Ge from the band basis functions at this point.[2,30] Compared with Ref. 18 where the effective electron masses are taken as granted, here we start from the free electron mass and straightforwardly obtain the renormalization of masses from this Hamiltonian. It can fit the band structure of the lowest three conduction bands and highest two valence bands, and provides the eigenstates for quantitative demonstration of conduction electron spin properties.

Till now, in addition to the well-known subgroup technique which gives the selection rules of the wave-vector-independent contribution to the electron-phonon interaction,[15,33–35] two approaches for deriving the explicit wave-vector dependence of scattering matrix have been brought forward.[18,32,36,37] In one approach the initial and final electronic states are expressed as the $\boldsymbol{k}\cdot\boldsymbol{p}$ eigenstates. The wave-vector dependence of scattering matrix element is the product of that in the electron/phonon states and crystal potential.[18,32] Here the selection rule for each analytical term is given by the group-theory analysis from the symmetries of the $\boldsymbol{k}\cdot\boldsymbol{p}$ basis functions, phonon state and crystal potential, while the coefficients of the electron-phonon scattering matrices are integrals involving the $\boldsymbol{k}\cdot\boldsymbol{p}$ basis functions and crystal potential and can be calculated straightforwardly via the pseudo-potential method. The other approach, i.e., the theory of invariants, utilizes the invariance of electron-phonon interaction to the symmetry operators in the corresponding space group.[30,31] The invariant scattering matrix consists of products of wave-vector-dependent irreducible tensor components and the bare spin-dependent matrices and takes into account the symmetry of phonon states. The corresponding coefficients should be obtained via calculation with numerical techniques such as pseudo-potential or tight-binding methods.[29–31,36,37] Obviously, the validity of the first approach is sensitive to the choice of $\boldsymbol{k}\cdot\boldsymbol{p}$ eigenstates, and the second one is not limited by the $\boldsymbol{k}\cdot\boldsymbol{p}$ Hamiltonian. Therefore we take the invariant method, and determine the coefficients via fitting with our pseudo-potential calculations.

By applying the method of invariants, we construct the scattering matrices and investigate the intra- and inter-valley scatterings involving both the Γ and four L valleys. The matrix elements for the intra-Γ and inter–Γ-L valley scattering, the OP contribution and separated transverse acoustic (TA) and longitudinal acoustic (LA) contributions to the intra-L valley electron-phonon scattering are provided for the first time. For each phonon mode, we demonstrate the lowest-order wave-vector dependence of the scattering matrix as it is much larger than the higher-order terms. It should be noted that the zeroth-order contribution to the spin-flip scattering elements does exist in the inter-valley scattering but vanishes in the intra-valley case. Furthermore, with our $\boldsymbol{k}\cdot\boldsymbol{p}$ Hamiltonian at the L point and a 14×14 $\boldsymbol{k}\cdot\boldsymbol{p}$ Hamiltonian at the Γ point, we analyze the Elliott[38] and Yafet[33] mechanisms in these electron-phonon scatterings.[39] In all the cases above, our calculations with pseudo-potential method confirm our selection rules and analytical wave-vector dependence of scattering matrices.

This paper is organized as follows. In Sec. II we construct the 16×16 $\boldsymbol{k}\cdot\boldsymbol{p}$ Hamiltonian. In Sec. III, we investigate the mechanisms of the phonon-induced electron scattering, where the intra-Γ/L valley scattering, inter–Γ-L valley scattering and inter–L-L valley scattering are studied analytically via the symmetry consideration. Besides, we calculate the scattering matrices numerically with pseudo-potential method. We summarize in Sec. IV.

II. THE $\boldsymbol{k}\cdot\boldsymbol{p}$ HAMILTONIAN

Around the conduction band minimum of Ge, the $\boldsymbol{k}\cdot\boldsymbol{p}$ Hamiltonian with the spin-orbit coupling included can be derived from the symmetry at the four L points $(\pi/a)(1,1,1)$, $(\pi/a)(-1,-1,1)$, $(\pi/a)(-1,1,1)$ and $(\pi/a)(1,-1,1)$ with a being the lattice constant. At each point, the symmetry of the Bloch states is described by the D_{3d} double group with the six irreducible representations L_4^+, L_5^+, L_6^+, L_4^-, L_5^- and L_6^-.[2,29,40] We first consider the vicinity of the $(\pi/a)(1,1,1)$ point. For the sake of convenience, we choose the coordinate system x, y, z with the z direction along the symmetry axis [111], so that the unit vectors of this system, related with those of the crystallographic frame [100], [010] and [001], i.e., $\hat{x}_0$, $\hat{y}_0$ and $\hat{z}_0$, by $\hat{x} = (\hat{x}_0-\hat{y}_0)/\sqrt{2}$, $\hat{y} = (\hat{x}_0+\hat{y}_0-2\hat{z}_0)/\sqrt{6}$ and $\hat{z} = (\hat{x}_0+\hat{y}_0+\hat{z}_0)/\sqrt{3}$. Starting from the nonrelativistic Bloch states $L_1, L_3, L_{3'}^c, L_{2'}$ in the conduction band and the $L_{3'}^v$ states in the valence band and including the spin-orbit interaction, we obtain 16 Bloch states given in Table IX of Appendix A, which are used in the construction of the $\boldsymbol{k}\cdot\boldsymbol{p}$ Hamiltonian and the analysis of the electron-phonon scattering.

Due to the space inversion symmetry in bulk Ge, the basis functions have defined parities. For this reason, the superscripts '+' and '−' are used to represent the even and odd parities, respectively. It is noted that all the bands are 2-fold degenerate due to the time inversion symmetry.[2] The spin-dependent perturbation Hamiltonian is given by[40,41]

$$\Delta H = \frac{\hbar}{4m_{\rm e}^2c^2}\left[\boldsymbol{\nabla}V(\boldsymbol{r})\times\boldsymbol{p}\right]\cdot\boldsymbol{\sigma} + \frac{\hbar\boldsymbol{k}\cdot\boldsymbol{\pi}}{m_{\rm e}} + \frac{\hbar^2k^2}{2m_{\rm e}}\ , \qquad (1)$$

in which $\boldsymbol{k}$ is the electron wave vector referred to the L-point, the first term describes the spin-orbit interaction at $\boldsymbol{k}=0$, m_e is the free electron mass, $V(\mathbf{r})$ is the spin-independent periodic potential and $\boldsymbol{\pi}$ is the generalized momentum operator[41]

$$\boldsymbol{\pi} = \boldsymbol{p} + \delta\boldsymbol{\pi}\ ,\ \delta\boldsymbol{\pi} = \frac{\hbar}{4m_ec^2}\boldsymbol{\sigma}\times\boldsymbol{\nabla}V(\boldsymbol{r})\ . \qquad (2)$$

The total $\boldsymbol{k}\cdot\boldsymbol{p}$ Hamiltonian matrix is written in the form of three terms

$$H = \frac{\hbar^2k^2}{2m_{\rm e}}\hat{I} + H_0 + H_{\boldsymbol{kp}}\ , \qquad (3)$$

where H_0 is the Hamiltonian matrix at the L-point and the $H_{\boldsymbol{kp}}$ is the linear-$\boldsymbol{k}$ contribution describing the interband $\boldsymbol{k}{\cdot}\boldsymbol{\pi}$ mixing. The diagonal components of H_0 are introduced in the third column of Table IX of Appendix A. The matrix H_0 also has off-diagonal components responsible for the interband spin-orbit mixing which takes place only between the band states transforming according to the equivalent spinor representations. The nonzero off-diagonal components which stem from $(\nabla V \times \mathbf{p}) \cdot \boldsymbol{\sigma}$ terms are

$$\langle v4|H_0|c12\rangle = \langle v3|H_0|c11\rangle = \Delta_1 \, , \tag{4a}$$

$$\langle c1|H_0|c4\rangle = \langle c2|H_0|c3\rangle = \Delta_2 \, , \tag{4b}$$

$$\langle c9|H_0|c11\rangle = \langle c10|H_0|c12\rangle = \Delta_3 \, , \tag{4c}$$

$$\begin{aligned} \langle v4|H_0|c10\rangle &= \langle v3|H_0|c9\rangle = -\langle v2|H_0|c8\rangle \\ &= -\langle v1|H_0|c7\rangle = \Delta_4 \end{aligned} \tag{4d}$$

together with 10 transposed matrix elements. Here Δ_l (l = 1, 2, 3, 4) are real band parameters and are listed in Table I.

The linear-$\boldsymbol{k}$ matrix can be rewritten as

$$H_{\boldsymbol{kp}} = \begin{bmatrix} H_{\rm cc} & H_{\rm vc}^{\dagger} \\ H_{\rm vc} & 0 \end{bmatrix} , \tag{5}$$

where $H_{\rm cc}$ and $H_{\rm vc}$ are 12×12 and 4×12 block submatrices, respectively. Taking into account that the matrix elements between the states of coinciding parities vanish, these submatrices can further be presented in the form

$$H_{\rm cc} = \begin{bmatrix} 0 & H_{\rm cc}^{+-} \\ H_{\rm cc}^{-+} & 0 \end{bmatrix} , \quad H_{\rm vc} = \begin{bmatrix} 0 & H_{\rm vc}^{-+} \end{bmatrix} , \tag{6}$$

where $H_{\rm cc}^{+-} = (H_{\rm cc}^{-+})^{\dagger}$. For the matrix elements of $\boldsymbol{k} \cdot \boldsymbol{p}$ one has

$$H_{\rm cc}^{-+}(\boldsymbol{k}\cdot\boldsymbol{p}) \;=\; \begin{pmatrix} P_6k_+ & -P_6k_- & Q_2k_+ & -Q_2k_- & 0 & P_5k_z \\ P_6k_+ & P_6k_- & -Q_2k_+ & -Q_2k_- & P_5k_z & 0 \\ -\sqrt{2}P_6k_- & 0 & 0 & -P_5k_z & -Q_2k_+ & -Q_2k_+ \\ 0 & \sqrt{2}P_6k_+ & -P_5k_z & 0 & -Q_2k_- & Q_2k_- \\ P_4k_z & 0 & 0 & \sqrt{2}P_3k_+ & P_3k_- & P_3k_- \\ 0 & P_4k_z & -\sqrt{2}P_3k_- & 0 & P_3k_+ & -P_3k_+ \end{pmatrix} \tag{7}$$

$$H_{\rm vc}(\boldsymbol{k}\cdot\boldsymbol{p}) \;=\; \begin{pmatrix} P_2k_z & 0 & -Q_1k_- & Q_1k_+ & P_1k_+ & -P_1k_- \\ 0 & P_2k_z & -Q_1k_- & -Q_1k_+ & P_1k_+ & P_1k_- \\ -Q_1k_+ & -Q_1k_+ & -P_2k_z & 0 & \sqrt{2}P_1k_- & 0 \\ Q_1k_- & -Q_1k_- & 0 & -P_2k_z & 0 & -\sqrt{2}P_1k_+ \end{pmatrix} \tag{8}$$

with $k_\pm = k_x \pm ik_y$. For the matrix $H_{\rm cc}^{-+}$, we use the "bra" and "ket" basis functions in the order $c6 \ldots c1$ and $c12 \ldots c7$ and, for the matrix $H_{\rm vc}^{-+}$, the "bra" basis functions are ordered from $v1$ to $v4$ and "ket" ones from $c6$ to $c1$. For the operator $\boldsymbol{k} \cdot \delta\boldsymbol{\pi}$, the matrix elements are as follows

$$H_{\rm cc}(\boldsymbol{k}\cdot\delta\boldsymbol{\pi}) = \begin{pmatrix} \alpha_6k_+ & -\alpha_6k_- & (\beta_2+\alpha_5)k_+ & (-\beta_2-\alpha_5)k_- & 0 & 2\sqrt{2}\beta_2k_z \\ \alpha_6k_+ & \alpha_6k_- & (-\beta_2+\alpha_5)k_+ & (-\beta_2+\alpha_5)k_- & -2\sqrt{2}\beta_2k_z & 0 \\ \sqrt{2}\alpha_6k_- & 2\sqrt{2}\alpha_6k_z & 0 & 0 & (\beta_2+\alpha_5)k_+ & (\beta_2-\alpha_5)k_+ \\ 2\sqrt{2}\alpha_6k_z & -\sqrt{2}\alpha_6k_+ & 0 & 0 & (\beta_2+\alpha_5)k_- & (-\beta_2+\alpha_5)k_- \\ 0 & \alpha_4k_+ & -2\sqrt{2}\alpha_3k_z & -\sqrt{2}\alpha_3k_+ & \alpha_3k_- & \alpha_3k_- \\ -\alpha_4k_- & 0 & \sqrt{2}\alpha_3k_- & -2\sqrt{2}\alpha_3k_z & \alpha_3k_+ & -\alpha_3k_+ \end{pmatrix} , \tag{9}$$

$$H_{\rm vc}(\boldsymbol{k}\cdot\delta\boldsymbol{\pi}) = \begin{pmatrix} 2\sqrt{2}\beta_1k_z & 0 & (\beta_1+\alpha_2)k_- & (-\beta_1-\alpha_2)k_+ & \alpha_1k_+ & -\alpha_1k_- \\ 0 & -2\sqrt{2}\beta_1k_z & (\beta_1-\alpha_2)k_- & (\beta_1-\alpha_2)k_+ & \alpha_1k_+ & \alpha_1k_- \\ (-\beta_1+\alpha_2)k_+ & (-\beta_1-\alpha_2)k_+ & 0 & 0 & -\sqrt{2}\alpha_1k_- & -2\sqrt{2}\alpha_1k_z \\ (\beta_1-\alpha_2)k_- & (-\beta_1-\alpha_2)k_- & 0 & 0 & -2\sqrt{2}\alpha_1k_z & \sqrt{2}\alpha_1k_+ \end{pmatrix} . \tag{10}$$

The coefficients $P_1, P_2 \ldots$ and $\alpha_1, \alpha_2 \ldots$ are purely imaginary and Q_1, Q_2, β_1, β_2 are real and are also listed in Table I. To illustrate the applied method to calculate the matrices (7)–(10), we consider the matrix elements between the L-point Bloch functions $\Psi_{j'} = L_4^-, L_5^-, L_{6(1)}^-, L_{6(2)}^-$ and $\Phi_j = L_4^+, L_5^+, L_{6(1)}^+, L_{6(2)}^+$, respectively for $j', j = 1, 2, 3, 4$, formed from the single-group states $L_{3'}$ and L_3 (See Table IX in Appendix A). Choosing the particular basis states $|L_{3'}, i'\rangle$ $(i' = 1, 2)$ and $|L_3, i\rangle$ $(i = 1, 2)$ we calculate, by using the symmetry considerations, the matrix elements of operators $\boldsymbol{k}\cdot\boldsymbol{p}$ and $U_\alpha = (\hbar^2/2m_ec^2)\left[\boldsymbol{\nabla}V(\boldsymbol{r})\times\boldsymbol{k}\right]_\alpha$ between them. Let us denote these matrix elements by M_{ij} and $U_{\alpha;ij}$. Now if we present the states $\Psi_{j'}$ and Φ_j as linear combinations $\sum_{i's'} C_{j',i's'}\alpha_{s'}\,|L_{3'}, i'\rangle$ and $\sum_{is} C_{j,is}\alpha_s\,|L_3, i\rangle$, where α_s is the spin-up state $\uparrow$ for $s = 1/2$ and spin-down state $\downarrow$ for $s = -1/2$, then the matrix elements between the spinor states are given by

$$\langle\Psi_{j'}|\boldsymbol{k}\cdot\boldsymbol{p}|\Phi_j\rangle = \sum_{i'is} C^*_{j',i's} M_{i'i} C_{j,is}\,,$$

$$\langle\Psi_{j'}|\boldsymbol{k}\cdot\delta\boldsymbol{\pi}|\Phi_j\rangle = \sum_{i'is's} C^*_{j',i's'}(\boldsymbol{U}_{i'i}\cdot\boldsymbol{\sigma}_{s's})C_{j,is}\,.$$

The zero point of wave vector is located at $(\pi/a)(1,1,1)$ point. $a = 5.66\,\text{Å}$ is the lattice constant of Ge.[2] One can see that the $\boldsymbol{k}\cdot\boldsymbol{p}$ and $(\nabla V\times\mathbf{k})\cdot\boldsymbol{\sigma}$ terms couple the bases with different parities and the $(\nabla V\times\mathbf{p})\cdot\boldsymbol{\sigma}$ terms connect bases with the same parity. We determine the $\boldsymbol{k}\cdot\boldsymbol{p}$ parameters (given in Table I) by fitting with an $sp^3d^5s^*$ tight-binding model.[27] One can see from Fig. 1 that the lowest three conduction bands and two highest valence bands calculated from the $\boldsymbol{k}\cdot\boldsymbol{p}$ parameters fit well with the tight-binding results.

For the other three L points, i.e., $(\pi/a)(-1,-1,1)$, $(\pi/a)(-1,1,1)$ and $(\pi/a)(1,-1,1)$, the basis functions and Hamiltonian share the same forms with those in Appendix A and Eqs. (5)-(10), while the coordinate system varies.

It is noted that a $\boldsymbol{k}\cdot\boldsymbol{p}$ matrix larger than or equal to 12×12 is necessary to fit the structure of the lowest conduction and highest valence bands without the remote-band influence. These bands are pertinent to the electron spin relaxation. Via the Löwdin partitioning,[40] the effective masses of i-th band can be expressed as

$$\frac{m_\mathrm{e}}{m_z^i} = 1 + \frac{2m_\mathrm{e}}{\hbar^2}\sum_{j\neq i}\frac{|H_{ij}|^2_{k_x,k_y=0}}{(E_i - E_j)k_z^2}, \tag{11a}$$

$$\frac{m_\mathrm{e}}{m_{x(y)}^i} = 1 + \frac{2m_\mathrm{e}}{\hbar^2}\sum_{j\neq i}\frac{|H_{ij}|^2_{k_z,k_y(k_x)=0}}{(E_i - E_j)k_{x(y)}^2}. \tag{11b}$$

For the lowest conduction band, $m_z = 1.36\,m_\mathrm{e}$, which confirms the importance of including the fourth conduction band.[27]

TABLE I: The parameters in the 16×16 $\mathbf{k}\cdot\mathbf{p}$ Hamiltonian in the vicinity of the L point. These parameters are obtained by fitting with the band structure in an $sp^3d^5s^*$ tight-binding model.[27]

	eV· nm		eV
Q_1	0.52	E_{v1}	−1.119
Q_2	0.26	E_{v2}	−1.365
P_1	$0.52\,i$	E_{c1}	0.747
P_2	$0.32\,i$	E_{c2}	3.990
P_3	$0.20\,i$	E_{c3}	4.110
P_4	$0.37\,i$	E_{c4}	8.349
P_5	$-0.35\,i$	E_{c5}	8.354
P_6	$-0.20\,i$	E_{c6}	9.109
β_1	0.03	Δ_1	0.012
β_2	0.01	Δ_2	0.089
α_1	$-0.01\,i$	Δ_3	0.041
α_2	$0.02\,i$	Δ_4	0.097
α_3	$0.02\,i$		
α_4	$0.52\,i$		
α_5	$0.04\,i$		
α_6	$0.02\,i$		

Moreover, with our 16×16 $\boldsymbol{k}\cdot\boldsymbol{p}$ Hamiltonian, it is easy to obtain the eigenstates of lowest conduction bands at the L points,

$$\begin{aligned}\varphi_{\frac{1}{2}} &= \frac{1}{A}[L^+_{6(1)}(L_1) - cL^+_{6(1)}(L_3)]\\ &= \frac{1}{A}[L_1\uparrow - c(L_{3y} - iL_{3x})\downarrow],\end{aligned} \tag{12a}$$

$$\begin{aligned}\varphi_{-\frac{1}{2}} &= \frac{1}{A}[L^+_{6(2)}(L_1) - cL^+_{6(2)}(L_3)]\\ &= \frac{1}{A}[L_1\downarrow + c(L_{3y} + iL_{3x})\uparrow],\end{aligned} \tag{12b}$$

where $L_{3x}\sim -zy$, $L_{3y}\sim zx$ and $\uparrow$ ($\downarrow$) is the spin up (down) eigenstate along the z direction in the corresponding coordinate system. A is the renormalization coefficient and c is a real parameter which can be calculated directly by diagonalizing the $\boldsymbol{k}\cdot\boldsymbol{p}$ Hamiltonian. Clearly the conduction electron states are spin-mixing at the L points. In this work the L_1, L_{3x} and L_{3y} are taken to be purely real.

III. ELECTRON-PHONON SCATTERING

We investigate the electron-phonon scatterings of L valleys and Γ valley in Ge, i.e., the intra-Γ/L valley, inter–Γ-L valley and inter-L valley scatterings. These

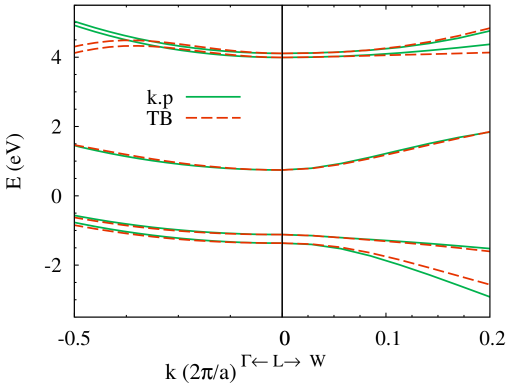

FIG. 1: (Color online) The lowest conduction bands and highest valence bands *vs.* wave vector near the $(\pi/a)(1,1,1)$ point. The origin of wave vector (the zero point in the figure) is taken to be at the $(\pi/a)(1,1,1)$ point. The green solid curves represent the result calculated via the $\boldsymbol{k}\cdot\boldsymbol{p}$ model and the red dashed curves describe the one obtained via the $sp^3d^5s^*$ tight-binding (TB) model.[27]

scatterings are fundamental to understand the spin dynamics in the optical orientation of spin and the hot-electron relaxation.[12,15,42,43] The complete scattering matrices and selection rules are determined with the invariant method and subgroup technique. Also, we analyze the Elliott[38] and Yafet[33] mechanisms in these electron-phonon scatterings facilitated by the $\boldsymbol{k}\cdot\boldsymbol{p}$ basis functions (See Table IX in Appendix A) and Hamiltonian obtained around the L point.[30,34,35] The coefficients in the scattering matrices are obtained by the pseudo-potential method, which further confirms our selection rules and wave-vector dependence.

We first derive the time-reversal constraint on the wave-vector dependence of scattering matrix. The spin-related scattering matrix in the centrosymmetric crystal can be generally written as

$$\hat{M}_{\mathbf{k},\mathbf{k}'} = A_{\mathbf{k},\mathbf{k}'}\hat{I} + \mathbf{B}_{\mathbf{k},\mathbf{k}'}\cdot\boldsymbol{\sigma}, \tag{13}$$

where $\mathbf{k}$ ($\mathbf{k}'$) is the wave vector of initial (final) electronic state and the spin eigenstates are along $\hat{z}$ direction. $\hat{I}$ is the 2×2 identity matrix and $\boldsymbol{\sigma}$ are the Pauli matrices. Via the time-reversal operator, it's easy to obtain the time-reversal constraint on the wave-vector dependence

$$A_{\mathbf{k},\mathbf{k}'} = A^{*}_{\mathbf{k}',\mathbf{k}} = A_{-\mathbf{k}',-\mathbf{k}}, \tag{14a}$$

$$\mathbf{B}_{\mathbf{k},\mathbf{k}'} = \mathbf{B}^{*}_{\mathbf{k}',\mathbf{k}} = -\mathbf{B}_{-\mathbf{k}',-\mathbf{k}}, \tag{14b}$$

where $A_{\mathbf{k},\mathbf{k}'}$ ($\mathbf{B}_{\mathbf{k},\mathbf{k}'}$) is purely real (imaginary).

Moreover, the spin-orientation dependence of the electron-phonon scattering can be obtained easily with this scattering matrix. The scattering elements with spin eigenstates along an arbitrary direction $\hat{n} = (\sin\theta\cos\phi, \sin\theta\sin\phi, \cos\theta)$ can be expressed as

$$\begin{aligned} M_{\mathbf{k},\mathbf{k}';\uparrow,\uparrow} =& A_{\mathbf{k},\mathbf{k}'} + \cos\theta B_{\mathbf{k},\mathbf{k}';z} \\ &+ \sin\theta(\cos\phi B_{\mathbf{k},\mathbf{k}';x} + \sin\phi B_{\mathbf{k},\mathbf{k}';y}), \end{aligned} \tag{15a}$$

$$\begin{aligned} M_{\mathbf{k},\mathbf{k}';\uparrow,\downarrow} =& -\sin\theta B_{\mathbf{k},\mathbf{k}';z} + (\cos\theta\cos\phi + i\sin\phi)B_{\mathbf{k},\mathbf{k}';x} \\ &+ (\cos\theta\sin\phi - i\cos\phi)B_{\mathbf{k},\mathbf{k}';y}. \end{aligned} \tag{15b}$$

We further analyze the wave-vector order of scattering matrix element, which is given by[15,32]

$$\begin{aligned} &\sqrt{\tfrac{\hbar}{2\rho V\omega_{\mathbf{q}}}}\sqrt{n_{\mathbf{q}} + \tfrac{1}{2} \pm \tfrac{1}{2}}M_{\mathbf{k},\mathbf{k}';s,s'} \\ &= \langle \mathbf{k}, s, n_{\mathbf{q}}|H_{\mathrm{ep}}|\mathbf{k}', s', n_{\mathbf{q}} \pm 1\rangle, \end{aligned} \tag{16}$$

with ρ, V, $\omega_{\mathbf{q}}$ and $n_{\mathbf{q}}$ representing the crystal mass density, crystal volume, phonon frequency and phonon occupation, respectively. The matrix element can be expressed in order of $\delta\mathbf{q} = (\mathbf{k}' - \mathbf{k}_{\mathrm{f}}) - (\mathbf{k} - \mathbf{k}_{\mathrm{i}})$,[15,32]

$$M_{\mathbf{k},\mathbf{k}';s,s'} = D_{0,s,s'} + \mathbf{D}_{1,s,s'}\cdot\delta\mathbf{q} + \delta\mathbf{q}\cdot\mathbf{D}_{2,s,s'}\cdot\delta\mathbf{q} + \ldots \tag{17}$$

with $\mathbf{k}_{\mathrm{i}}$ ($\mathbf{k}_{\mathrm{f}}$) being the valley center of the initial (final) state and $\delta\mathbf{q} \ll 2\pi/a$.[44] There are vanishing (non-vanishing) zeroth-order contributions to the spin-flip scattering in the intra- (inter-) valley scatterings. Hereafter we derive the lowest-order wave-vector dependence of the scattering matrix for each phonon mode only due to its dominant contribution compared to the corresponding higher order terms. We also give the non-zeroth order contributions to the spin-flip intervalley electron-phonon scatterings in the spherical-band-approximation for completeness.

TABLE II: Phonon polarization vectors in the long-wavelength limit ($\mathbf{q} \ll 2\pi/a$). Here the superscript "+" ("−") represents the in-phase (out-of-phase). We have used the elastic continuum approximation for diamond crystal structures. Two TA or TO polarizations can be linearly combined into any other orthonormal ones.

$\xi^{+}_{\mathrm{TA}_1}, \xi^{-}_{\mathrm{TO}_1}(\mathbf{q})$	$(q_y, -q_x, 0)/\sqrt{q_x^2 + q_y^2}$
$\xi^{+}_{\mathrm{TA}_2}, \xi^{-}_{\mathrm{TO}_2}(\mathbf{q})$	$(q_xq_z, q_yq_z, -q_x^2 - q_y^2)/(\sqrt{q_x^2 + q_y^2}\lvert\mathbf{q}\rvert)$
$\xi^{+}_{\mathrm{LA}}, \xi^{-}_{\mathrm{LO}}(\mathbf{q})$	$\mathbf{q}/\lvert\mathbf{q}\rvert$

A. Numerical method

To obtain the coefficients of these scattering matrices, we derive the electron-phonon interaction and evaluate the matrix elements under an empirical pseudo-potential model by following Ref. [45]. This method has been successfully used in the calculation of the spin relaxation time,[46] the degree of circular polarization of the luminescence across the indirect band[47] and indirect optical injections[45] in bulk Si, and obtains good agreements with experiments. In this model, the real single particle potential $V(\boldsymbol{r}) = \sum_{i\alpha} v(\boldsymbol{r} - \boldsymbol{R}_{i\alpha})$ is replaced by a smooth pseudo potential $\tilde{v}(\boldsymbol{r}) = v_L(\boldsymbol{r}) + v_{NL}(\boldsymbol{r}) + v_{so}(r)\boldsymbol{l} \cdot \boldsymbol{\sigma}$ which includes the local potential v_L, the non-local one v_{NL}, and the spin-orbit coupling part v_{so} with $\boldsymbol{l}$ being the orbital momentum operator. Here the subscripts i and α are the indices for the primitive cells of the crystal and atoms in a primitive cell separately. This pseudo potential is chosen to produce the same single particle energy as the real potential but a much smooth wave function around the nuclei. Therefore, the choice of the pseudo potential is not unique. In our calculation, it is taken from Ref. [48]. The calculated electron energies at the band edges of conduction band for Γ and L valleys match those in the $sp^3d^5s^*$ tight-binding model.[27] By shifting the atom position $\boldsymbol{R}_{i\alpha}$ by $\boldsymbol{u}_{i\alpha}$ and expanding $V(\boldsymbol{r})$ with respect to $\boldsymbol{u}_{i\alpha}$, the linear term in the expansion is the electron-phonon interaction H_{ep}. The atom displacement is related to phonon operators by $\boldsymbol{u}_{i\alpha} = \sum_{\boldsymbol{q}\lambda}(\hbar/\rho\omega_{\boldsymbol{q}})^{1/2}(a_{\boldsymbol{q}\lambda} + a^{\dagger}_{-\boldsymbol{q}\lambda})\boldsymbol{\epsilon}^{\alpha}_{\boldsymbol{q}\lambda}e^{i\boldsymbol{q}\cdot\boldsymbol{R}_i}$, where $\boldsymbol{q}/\lambda$ represents the phonon wave vector/mode. We calculate the phonon polarization vectors $\boldsymbol{\epsilon}_{\boldsymbol{q}\lambda}$ by an adiabatic bond charge model.[49] The calculated energies for the phonons involved in the scattering channels studied here are 10.2, 28.6 and 33.3 meV for X_3, X_1 and X_4 phonons, and 7.4, 25.6, 29.3 and 35.80 meV for L_3, $L_{2'}$, L_1 and $L_{3'}$ phonons, respectively.

With the pseudo-potential method, we obtain the electron-phonon matrix elements for the intra-Γ/L valley, inter–Γ-L valley and inter-L valley scatterings in Ge, and confirm the selection rules and scattering matrices in all cases. The coefficients in these scattering matrices are determined by fitting with the pseudo-potential results and are listed in Tables III-VII. One can see that generally the scattering matrix element for the spin-conserving process scattering is much larger (more than 50 times) than that for the spin-flip one.

B. Intravalley scattering

We first address the intra-Γ/L valley electron-phonon scatterings in Ge with the theory of invariants, where the LA, TA and OP contributions are all included.[30,31] The contributions of two TA (three OP) phonon modes are summed up as their sound velocities (phonon energies) near the Γ point are close to each other.[32] It should be noted that, beyond the symmetry of each phonon branch, the wave-vector dependence of polarization vectors for AC (belong to Γ^-_{15} irreducible representation) and OP (belong to Γ^+_{25} irreducible representation) phonon modes at the Γ point are well-known and compact (See Table II), which facilitate our derivation of the wave-vector dependence of the matrix elements. In Ge, the wave-vector-order analysis of the spin-flip process has already been performed based on the time-reversal and space-inversion symmetry, where the leading-order terms for the AC phonons are third-order ($K_l q_m q_n$) and those for the OPs are second-order ($K_l q_m$) ($l, m, n \in \{x, y, z\}$).[18,32,33]

1. *Intra-Γ valley scattering*

In intra-Γ scattering case, we apply the conventional coordinate system for simplify. The $\hat{M}_{\mathbf{k},\mathbf{k}'}$ should be an invariant in O_h point group.[2,29] First, one can see that the zeroth-order contribution of scattering matrix vanishes as

$$\Gamma^-_7 \otimes \Gamma^-_7 = \Gamma^+_1 + \Gamma^+_{15}. \tag{18}$$

TABLE III: The nonvanishing coefficients in the intra-Γ valley electron-phonon scattering matrix. The first two columns are the coefficients for the AC phonons, and the last two columns show the parameters in the OP case. $\Xi_1 = 8.42$ eV is the coefficient for the LA contribution to the spin-conserving scattering.

	AC, eV·nm^2	OP, eV· nm
R_1	-0.61	
R_2	0.55	4.35
R_3	0.60	
R_4	-0.83	
R_5	-1.19	0.0055
R_6	2.00	0.35

For the O_h point group, the symmetries of spin-dependent matrices are given by

$$\hat{I} \sim \Gamma^+_1, \qquad \boldsymbol{\sigma} \sim \Gamma^+_{15}. \tag{19}$$

Therefore, from the invariance of the scattering matrix $\hat{M}_{\mathbf{k},\mathbf{k}'}$, the symmetries of $A_{\mathbf{k},\mathbf{k}'}$ and $\mathbf{B}_{\mathbf{k},\mathbf{k}'}$ can be determined by

$$A_{\mathbf{k},\mathbf{k}'} \sim \Gamma^+_1, \qquad \mathbf{B}_{\mathbf{k},\mathbf{k}'} \sim \Gamma^+_{15}. \tag{20}$$

Then we can construct their explicit forms, which are functions of the wave vectors and phonon polarization vectors. It should be noted that the time-reversal constraint [Eq. (14)] must be fulfilled. The symmetry-allowed terms are given by

$$A_{\mathbf{k},\mathbf{k}'} = \Xi_1(u_{xx} + u_{yy} + u_{zz}) \tag{21}$$

$$\mathbf{B}_{\mathbf{k},\mathbf{k}'} = i\sum_{j=1}^{6} R_j \mathbf{S}^{(j)}_{\mathbf{k},\mathbf{k}'}, \tag{22}$$

with

$$S_z^{(1)} = (\mathbf{K}\times\mathbf{q})_z(u_{xx}+u_{yy}+u_{zz}), \tag{23a}$$

$$S_z^{(2)} = (\mathbf{K}\times\mathbf{q})_x u_{zx} + (\mathbf{K}\times\mathbf{q})_y u_{yz}, \tag{23b}$$

$$S_z^{(3)} = (\mathbf{K}\times\mathbf{q})_z u_{zz}, \tag{23c}$$

$$S_z^{(4)} = (K_x q_y + K_y q_x)(u_{xx}-u_{yy}), \tag{23d}$$

$$S_z^{(5)} = (K_y q_z + K_z q_y)u_{zx} - (K_z q_x + K_x q_z)u_{yz}, \tag{23e}$$

$$S_z^{(6)} = (K_x q_x - K_y q_y)u_{xy}. \tag{23f}$$

Here we omit the subscripts $\mathbf{k},\mathbf{k}'$ for simplicity in Eqs. (23a)-(23f). The components of $\mathbf{S}_{\mathbf{k},\mathbf{k}'}$ are connected by the coordinate permutation. $\mathbf{K} = \mathbf{k}' + \mathbf{k}$ and $\mathbf{q} = \mathbf{k}' - \mathbf{k} = \delta\mathbf{q}$. $\mathbf{K}$ and $\mathbf{q}$ are in the same order. For AC modes, $u_{\alpha\beta} = \frac{1}{2}(q_\alpha \xi^+_{\mathrm{ac},\beta} + q_\beta \xi^+_{\mathrm{ac},\alpha})$ with α $(\beta) \in \{x,y,z\}$. In OP modes, we set $u_{\alpha\alpha} = 0$ and replace u_{yz}, u_{zx}, u_{xy} by optical vibration amplitudes $\xi^-_{\mathrm{op},x}, \xi^-_{\mathrm{op},y}, \xi^-_{\mathrm{op},z}$. Here $\boldsymbol{\xi}^+_{\mathrm{ac}}$ and $\boldsymbol{\xi}^-_{\mathrm{op}}$ are the phonon polarization vectors in the long-wavelength limit, which are given in Table II. The coefficients Ξ_i and R_i are listed in Table III.

Finally, from the numerical pseudo-potential calculation, we can see that for the spin-conserving scattering, the scattering element for LA phonon branch is more than 2 orders of magnitude larger than that for other modes, as the lowest order spin-conserving element only exists in LA case [See Eq. (21)]. While for the spin-flip scattering, the OP contribution is about 4 orders of magnitude larger than the AC contribution.

2. *Intra-L valley scattering*

Recently, Tang *et al.*[15] and Li *et al.*[18] investigated the intra-L electron-phonon scattering in Ge both analytically and numerically. Tang *et al.*[15] gave the average absolute values of the scattering elements for the AC contribution, and for the spin-conserving process of the OP contribution in the spherical-band-approximation. Li *et al.*[18] derived the approximated wave-vector dependence for the AC contribution, where the contributions of the three AC phonon modes were summed up. Here we demonstrate the complete and detailed wave-vector dependence for the intra-L valley scattering matrix via the theory of invariants, where the LA, TA and OP contributions are all considered.

In the intra-L valley scattering, the scattering matrix $\hat{M}_{\mathbf{k},\mathbf{k}'}$ should be an invariant in the D_{3d} point group.[2,29] We consider the $(\pi/a)(1,1,1)$ point and choose the [111] coordinate system for simplicity. The results in other three L points can be obtained by coordinate rotation. Here $\mathbf{k}_\mathrm{i} = \mathbf{k}_\mathrm{f} = (\pi/a)(1,1,1)$ and should be extracted from the initial and final wave-vectors. In this case, the zeroth-order contribution of the OP modes to spin-conserving scattering exists,

$$L_6^+ \otimes L_6^+ = \Gamma_1^+ + \Gamma_{25}^+, \tag{24}$$

and the zeroth-order spin-flip elements are forbidden by time-reversal symmetry.[15]

For D_{3d} point group, the symmetries of the spin-dependent matrices are reduced to

$$\hat{I} \sim L_1, \qquad \sigma_z \sim L_2, \qquad (\sigma_x, \sigma_y) \sim (L_{3x}, L_{3y}). \tag{25}$$

To ensure the invariance of $\hat{M}_{\mathbf{k},\mathbf{k}'}$, the symmetries of the $A_{\mathbf{k},\mathbf{k}'}$ and $\mathbf{B}_{\mathbf{k},\mathbf{k}'}$ are given by

$$A_{\mathbf{k},\mathbf{k}'} \sim L_1, \qquad B_{\mathbf{k},\mathbf{k}';z} \sim L_2, \tag{26}$$

$$(B_{\mathbf{k},\mathbf{k}';x}, B_{\mathbf{k},\mathbf{k}';y}) \sim (L_{3x}, L_{3y}). \tag{27}$$

Then, the explicit wave-vector of the scattering matrix can be constructed as well, which is much more complex than that in intra-Γ case as the symmetry is reduced.

$$A_{\mathbf{k},\mathbf{k}'} = \Xi_1(u_{xx}+u_{yy}) + \Xi_2 u_{zz}, \tag{28}$$

$$B_{\mathbf{k},\mathbf{k}';z} = i\sum_{j=1}^{8} C_j S^{(j)}_{\mathbf{k},\mathbf{k}';z}, \tag{29}$$

$$(B_{\mathbf{k},\mathbf{k}';x}, B_{\mathbf{k},\mathbf{k}';y}) = i\sum_{j=1}^{18} R_j (S^{(j)}_{\mathbf{k},\mathbf{k}';x}, S^{(j)}_{\mathbf{k},\mathbf{k}';y}), \tag{30}$$

with

$$S_z^{(1)} = (u_{xx}+u_{yy})(\mathbf{K}\times\mathbf{q})_z, \tag{31a}$$

$$S_z^{(2)} = u_{zz}(\mathbf{K}\times\mathbf{q})_z, \tag{31b}$$

$$\begin{aligned} S_z^{(3)} &= 2u_{xy}(q_x K_x - q_y K_y) \\ &\quad - (u_{xx}-u_{yy})(q_x K_y + q_y K_x), \end{aligned} \tag{31c}$$

$$S_z^{(4)} = q_z[(u_{xx}-u_{yy})K_x - 2u_{xy}K_y], \tag{31d}$$

$$S_z^{(5)} = K_z[(u_{xx}-u_{yy})q_x - 2u_{xy}q_y], \tag{31e}$$

$$S_z^{(6)} = u_{yz}(K_x q_y + K_y q_x) - u_{xz}(K_x q_x - K_y q_y), \tag{31f}$$

$$S_z^{(7)} = q_z(u_{xz}K_y - u_{yz}K_x), \tag{31g}$$

$$S_z^{(8)} = K_z(u_{xz}q_y - u_{yz}q_x), \tag{31h}$$

and

$$(S_x^{(1)}, S_y^{(1)}) = (u_{xx} + u_{yy})q_z(-K_y, K_x), \tag{32a}$$

$$(S_x^{(2)}, S_y^{(2)}) = u_{zz}q_z(-K_y, K_x), \tag{32b}$$

$$(S_x^{(3)}, S_y^{(3)}) = (u_{xx} + u_{yy})K_z(-q_y, q_x), \tag{32c}$$

$$(S_x^{(4)}, S_y^{(4)}) = u_{zz}K_z(-q_y, q_x), \tag{32d}$$

$$\begin{aligned}(S_x^{(5)}, S_y^{(5)}) = {}& (u_{xx} + u_{yy})(q_xK_x - q_yK_y, \\ & - q_yK_x - q_xK_y),\end{aligned} \tag{32e}$$

$$(S_x^{(6)}, S_y^{(6)}) = u_{zz}(q_xK_x - q_yK_y, -q_yK_x - q_xK_y), \tag{32f}$$

$$(S_x^{(7)}, S_y^{(7)}) = q_zK_z(u_{xx} - u_{yy}, -2u_{xy}), \tag{32g}$$

$$(S_x^{(8)}, S_y^{(8)}) = (q_xK_x + q_yK_y)(u_{xx} - u_{yy}, -2u_{xy}), \tag{32h}$$

$$(S_x^{(9)}, S_y^{(9)}) = q_zK_z(-u_{yz}, u_{xz}), \tag{32i}$$

$$(S_x^{(10)}, S_y^{(10)}) = (q_xK_x + q_yK_y)(-u_{yz}, u_{xz}), \tag{32j}$$

$$\begin{aligned}(S_x^{(11)}, S_y^{(11)}) = {}& [(u_{xx} - u_{yy})(q_xK_x - q_yK_y) \\ & - 2u_{xy}(q_xK_y + q_yK_x), \\ & (u_{xx} - u_{yy})(q_xK_y + q_yK_x) \\ & + 2u_{xy}(q_xK_x - q_yK_y)],\end{aligned} \tag{32k}$$

$$\begin{aligned}(S_x^{(12)}, S_y^{(12)}) = {}& [u_{xz}(q_xK_y + q_yK_x) \\ & - u_{yz}(q_xK_x - q_yK_y), \\ & - u_{xz}(q_xK_x - q_yK_y) \\ & - u_{yz}(q_xK_y + q_yK_x)],\end{aligned} \tag{32l}$$

$$\begin{aligned}(S_x^{(13)}, S_y^{(13)}) = {}& K_z[(u_{xx} - u_{yy})q_y - 2u_{xy}q_x, \\ & (u_{xx} - u_{yy})q_x + 2u_{xy}q_y],\end{aligned} \tag{32m}$$

$$\begin{aligned}(S_x^{(14)}, S_y^{(14)}) = {}& q_z[(u_{xx} - u_{yy})K_y - 2u_{xy}K_x, \\ & (u_{xx} - u_{yy})K_x + 2u_{xy}K_y],\end{aligned} \tag{32n}$$

$$(S_x^{(15)}, S_y^{(15)}) = K_z(u_{yz}q_y - u_{xz}q_x, u_{yz}q_x + u_{xz}q_y), \tag{32o}$$

$$(S_x^{(16)}, S_y^{(16)}) = q_z(u_{yz}K_y - u_{xz}K_x, u_{yz}K_x + u_{xz}K_y), \tag{32p}$$

$$(S_x^{(17)}, S_y^{(17)}) = (\mathbf{K} \times \mathbf{q})_z(2u_{xy}, u_{xx} - u_{yy}), \tag{32q}$$

$$(S_x^{(18)}, S_y^{(18)}) = (\mathbf{K} \times \mathbf{q})_z(u_{xz}, u_{yz}). \tag{32r}$$

Here we have again omitted the subscripts $\mathbf{k}, \mathbf{k}'$ in Eqs. (31a)-(32r). The components of $\mathbf{S}_{\mathbf{k},\mathbf{k}'}$ cannot be connected by the coordinate permutation now due to the reduced symmetry. Here $u_{xx} + u_{yy}$ corresponds to $\xi^-_{\mathrm{op},z}$ for OP modes, and other expressions are the same as those in the intra-Γ case. It should be noted that the quadratic sum of OP contributions of $A_{\mathbf{k},\mathbf{k}'}$ is constant [See Eq. (28)] and Table II, which is in agreement with the selection rule [Eq. (24)]. Moreover, Eqs. (31a), (31b) and (32c)-(32f) are in agreement with the approximated analytical forms of the intra-L scattering matrix in Li's work.[18] Obviously our wave-vector-dependent scattering matrices are more detailed than those in previous works.[15,18]

Finally the coefficients Ξ_i, C_i and R_i in the intra-L valley electron-phonon scattering matrix are calculated from the pseudo-potential calculation with the non-vanishing ones listed in Table IV. It is interesting to see that for the spin-conserving scattering, unlike the intra-Γ case, the LA contribution is close to the TA one, as the lowest-order spin-conserving elements exist in both cases. For the spin-flip scattering, the ratio of OP contribution and AC contribution is close to that in intra-Γ case. Our AC contribution and the spin-conserving OP contribution are in the same order as those in previous work.[15,18]

TABLE IV: The nonvanishing coefficients in the intra-L valley electron-phonon scattering matrix. The first two columns are the coefficients for AC phonon modes and the last two columns show that in OP case.

AC	eV	OP	eV/nm
Ξ_1	-8.6	Ξ_1	43.8
Ξ_2	5.8		
AC	eV·nm^2	OP	eV·nm
R_1	-3.5×10^{-3}	R_1	6.0×10^{-3}
R_2	2.1×10^{-3}	R_3	-2.0×10^{-2}
R_3	4.2×10^{-3}	R_5	1.3×10^{-2}
R_4	0.5×10^{-4}	R_9	6.9×10^{-3}
R_5	2.0×10^{-3}	R_{10}	-2.8×10^{-2}
R_6	3.5×10^{-3}	R_{12}	-6.5×10^{-2}
R_7	-1.0×10^{-5}	R_{15}	2.5×10^{-2}
R_8	-1.2×10^{-3}	R_{16}	-1.8×10^{-2}
R_9	-5.9×10^{-4}	R_{18}	-7.0×10^{-2}
R_{10}	1.0×10^{-2}		
R_{11}	-6.0×10^{-4}		
R_{12}	-4.9×10^{-3}		
R_{13}	3.3×10^{-3}		
R_{14}	5.0×10^{-3}		
R_{15}	2.0×10^{-3}		
R_{16}	8.6×10^{-4}		
R_{17}	-2.5×10^{-3}		
R_{18}	-2.0×10^{-3}		
C_1	-5.6×10^{-2}	C_2	1.45×10^{-1}
C_2	-4.8×10^{-2}	C_6	6.0×10^{-2}
C_3	1.2×10^{-1}	C_7	-8.0×10^{-3}
C_4	6.0×10^{-3}	C_8	1.62×10^{-2}
C_5	8.6×10^{-3}		
C_6	-2.0×10^{-2}		
C_7	-6.0×10^{-4}		
C_8	-2.6×10^{-3}		

C. Intervalley scattering

1. *Inter–Γ-L valley scattering*

In this part we investigate the inter–Γ-L valley electron-phonon scattering. As pointed out by Li *et al.*,[19] the zeroth-order scattering matrix elements of both the spin-conserving and spin-flip processes exist. Thus we first focus on the analysis of the zeroth-order contributions with subgroup techniques.[34,35] We then investigate the other lowest-order non-vanishing wave-vector dependence of the scattering induced by each phonon branch with the method of invariants.[31]

Obviously the scatterings to the four L valleys are equivalent in unstrained bulk Ge except for the coordinate rotation. Here we consider the $(\pi/a)(1,1,1)$ valley and choose the [111] coordinate system. The lowest conduction bands at the Γ point are basis functions of the Γ_7^- irreducible representation,[2]

$$\Gamma^-_{7(1)} = \Gamma^-_2 \uparrow, \qquad \Gamma^-_{7(2)} = \Gamma^-_2 \downarrow, \tag{33}$$

where the spin eigenstates are along the $\hat{z}$ direction. The eigenstates of conduction band minima at the L point are given in Eq. (12), which are spin-mixed. Besides, the phonon states at the L point, which correspond the inter–Γ-L valley scattering, are basis functions of L_3, $L_{2'}$, L_1 and $L_{3'}$ irreducible representations.[2]

The symmetry of the inter–Γ-L valley scattering is described by the D_{3d} point group,[2,29] where the symmetry of the wave-vectors is given by

$$K_z \sim L_{2'},\ (K_x, K_y) \sim L_{3'},\ q_z \sim L_{2'},\ (q_x, q_y) \sim L_{3'}. \tag{34}$$

Here $\mathbf{K} = \mathbf{k}' - \mathbf{k}_L + \mathbf{k} - \mathbf{k}_\Gamma$ and $\mathbf{q} = \mathbf{k}' - \mathbf{k}_L - (\mathbf{k} - \mathbf{k}_\Gamma)$ with $\mathbf{k}_\Gamma = (\pi/a)(0,0,0)$ and $\mathbf{k}_L = (\pi/a)(1,1,1)$. By subgroup techniques, we obtain a general selection rule,[34,35]

$$L_6^+ \otimes \Gamma_7^- = L_{1'} + L_{2'} + L_{3'}. \tag{35}$$

Thus only the zeroth-order contributions from the $L_{2'}$ and $L_{3'}$ phonons exist.

We then give a more detailed symmetry analysis on the zeroth-order contributions. There are various electron-phonon mechanisms as the L_6^+, Γ_7^- and $L_{3'}$ states are all two-fold degenerate. In each particular case, we perform the operators in D_{3d} point group on the initial, final and phonon states. We find that many elements are forbidden, and there are relations between the nonvanishing elements

$$\langle \Gamma^-_{7(1)} | V_{L_{2'}} | L^+_{6(1)} \rangle \overset{C_{2(1)}}{=} \langle \Gamma^-_{7(2)} | V_{L_{2'}} | L^+_{6(2)} \rangle, \tag{36}$$

$$\langle \Gamma^-_{7(1)} | V_{L_{3'(2)}} | L^+_{6(2)} \rangle \overset{C_{2(1)}}{=} -\langle \Gamma^-_{7(2)} | V_{L_{3'(1)}} | L^+_{6(1)} \rangle, \tag{37}$$

in which $C_{2(1)}$ stands for the rotation around the $\hat{x}$ direction for π. $L_{3'(1)}$ and $L_{3'(2)}$ [$L^+_{6(1)}$ and $L^+_{6(2)}$] are basis functions of the $L_{3'}$ (L_6^+) irreducible representation, which are given in Appendix A. One can see that for spin eigenstates along the $\hat{z}$ direction, only the $L_{2'}$ ($L_{3'}$) phonon branch contributes to the spin-conserving (spin-flip) scattering, which is in agreement with the selection rules in the previous work.[19] With Eq. (37) and the time-revesal symmetry [See Eqs. (13) and (14)], we obtain an additional limit on the $L_{3'}$ contribution

$$\begin{aligned} & B_{\mathbf{k}_\Gamma,\mathbf{k}_L;x}(L_{3'}) - iB_{\mathbf{k}_\Gamma,\mathbf{k}_L;y}(L_{3'}) \\ &= -B_{\mathbf{k}_\Gamma,\mathbf{k}_L;x}(L_{3'}) - iB_{\mathbf{k}_\Gamma,\mathbf{k}_L;y}(L_{3'}). \end{aligned} \tag{38}$$

Thus the inter–Γ-L valley scattering matrix can be expressed as

$$\hat{M}_{\mathbf{k}_\Gamma,\mathbf{k}_L} = \begin{pmatrix} A_{\mathbf{k}_\Gamma,\mathbf{k}_L}(L_{2'}) & -iB_{\mathbf{k}_\Gamma,\mathbf{k}_L;y}(L_{3'(2)}) \\ iB_{\mathbf{k}_\Gamma,\mathbf{k}_L;y}(L_{3'(1)}) & A_{\mathbf{k}_\Gamma,\mathbf{k}_L}(L_{2'}) \end{pmatrix}, \tag{39}$$

with

$$B_{\mathbf{k}_\Gamma,\mathbf{k}_L;y}(L_{3'(2)}) = B_{\mathbf{k}_\Gamma,\mathbf{k}_L;y}(L_{3'(1)}) = B_{\mathbf{k}_\Gamma,\mathbf{k}_L;y}(L_{3'}), \tag{40}$$

where $A_{\mathbf{k}_\Gamma,\mathbf{k}_L}(L_{2'})$ [$B_{\mathbf{k}_\Gamma,\mathbf{k}_L;y}(L_{3'})$] is purely real (imaginary). The coefficients are given in Table V. It should be noted that the two non-diagonal terms come from two different $L_{3'}$ basis functions separately, which makes the spin-orientation dependence of scattering matrix in this case different from the general form in Eq. (15).

Now we consider the spin-orientation dependence of the inter–Γ-L valley scattering, which is given by

$$\begin{aligned} |M_{\mathbf{k}_\Gamma,\mathbf{k}_L;\uparrow,\uparrow}|^2 &= |M_{\mathbf{k}_\Gamma,\mathbf{k}_L;\uparrow,\uparrow}(L_{2'})|^2 + |M_{\mathbf{k}_\Gamma,\mathbf{k}_L;\uparrow,\uparrow}(L_{3'})|^2 \\ &= |A_{\mathbf{k}_\Gamma,\mathbf{k}_L}(L_{2'})|^2 \\ &\quad + \left| -\frac{i}{2}\sin\theta e^{-i\phi} B_{\mathbf{k}_\Gamma,\mathbf{k}_L;y}(L_{3'(2)}) \right|^2 \\ &\quad + \left| -\frac{i}{2}\sin\theta e^{i\phi} B_{\mathbf{k}_\Gamma,\mathbf{k}_L;y}(L_{3'(1)}) \right|^2 \\ &= |A_{\mathbf{k}_\Gamma,\mathbf{k}_L}(L_{2'})|^2 + \frac{1}{2}\sin^2\theta |B_{\mathbf{k}_\Gamma,\mathbf{k}_L;y}(L_{3'})|^2, \end{aligned} \tag{41}$$

$$\begin{aligned} |M_{\mathbf{k}_\Gamma,\mathbf{k}_L;\uparrow,\downarrow}|^2 &= |M_{\mathbf{k}_\Gamma,\mathbf{k}_L;\uparrow,\downarrow}(L_{2'})|^2 + |M_{\mathbf{k}_\Gamma,\mathbf{k}_L;\uparrow,\downarrow}(L_{3'})|^2 \\ &= \left| i\sin^2\frac{\theta}{2} e^{i\phi} B_{\mathbf{k}_\Gamma,\mathbf{k}_L;y}(L_{3'(2)}) \right|^2 \\ &\quad + \left| i\cos^2\frac{\theta}{2} e^{-i\phi} B_{\mathbf{k}_\Gamma,\mathbf{k}_L;y}(L_{3'(1)}) \right|^2 \\ &= \frac{1+\cos^2\theta}{2} |B_{\mathbf{k}_\Gamma,\mathbf{k}_L;y}(L_{3'})|^2, \end{aligned} \tag{42}$$

where ↑ (↓) is the spin eigenstate along an arbitrary direction $\hat{n} = (\sin\theta\cos\phi, \sin\theta\sin\phi, \cos\theta)$. One can see that generally both the $L_{2'}$ and $L_{3'}$ phonons are involved in the spin-conserving scattering and only the $L_{3'}$ one contributes to the spin-flip process. The spin-flip scattering shows obvious spin-orientation dependence, where the scattering is strongest (weakest) with the spin eigenstates along (perpendicular to) the $\hat{z}$ direction. This anisotropy will be weakened when considering the other three channels of inter–Γ-L valley scatterings, which can be obtained by the coordinate rotations. Numerically, the spin-conserving coefficient $|A_{\mathbf{k}_\Gamma,\mathbf{k}_L}(L_{2'})|$ is much larger (about 50 times) than the spin-flip one $|B_{\mathbf{k}_\Gamma,\mathbf{k}_L;y}(L_{3'})|$ (See Table V), and therefore the spin-conserving scattering is nearly isotropic.

TABLE V: The coefficients in the inter–Γ-L valley electron-phonon scattering matrix and the first- and second-order contributions to the spin-flip process in the spherical band-approximation. $A_{\mathbf{k}_\Gamma,\mathbf{k}_L}$ and $B_{\mathbf{k}_\Gamma,\mathbf{k}_L;y}$ represent the values for the zeroth-order contributions to the scattering matrix. R_i and Ξ_i are the coefficients of the first-order terms in the scattering matrices, and C_i denote the parameters of the second-order ones. D_1 and D_2 are the parameters of the first- and second-order contributions to the spin-flip process in the spherical-band approximation, with the spin eigenstates along the [111] direction.

eV/nm		eV	
$A_{\mathbf{k}_\Gamma,\mathbf{k}_L}(L_{2'})$	18.21	R_1	0.73
$iB_{\mathbf{k}_\Gamma,\mathbf{k}_L;y}(L_{3'})$	0.35	R_2	-0.34
		R_3	-2.15×10^{-2}
		R_4	2.46×10^{-2}
		R_5	37.64×10^{-2}
		R_6	-38.23×10^{-2}
		R_7	1.66
		R_8	-2.06

eV		eV·Å	
Ξ_1	12.0	C_1	12.7
Ξ_2	-9.15	C_2	4.54
Ξ_3	-30.5	C_3	6.04
Ξ_4	20.5	C_4	2.51
$D_1(L_3)$	2.79×10^{-3}	C_5	-15.5
$D_1(L_1)$	2.14×10^{-1}	C_6	4.16
		C_7	7.08
		C_8	-3.98
		$D_2(L_{2'})$	0.54

As the zeroth-order terms of the contributions of the L_3/L_1 phonon and the spin-flip process of the $L_{2'}$ phonon are absent, we further derive the lowest-order non-vanishing wave-vector dependence of these contributions with the method of invariants. From the space-inversion symmetry of the electron/phonon states and the wave-vectors [See Eq. (34)], one finds that the L_3/L_1 ($L_{2'}$) phonons only contribute to the odd- (even-)order terms in the scattering matrix. For the L_3/L_1 phonons, the first-order terms exist in both the spin-conserving and spin-flip processes, given by

$$A(L_{3x}) = -i(\Xi_1 q_y + \Xi_2 K_y), \tag{43a}$$
$$B_z(L_{3x}) = R_1 q_x + R_2 K_x, \tag{43b}$$
$$B_x(L_{3x}) = -(R_3 q_y + R_4 K_y - R_5 q_z - R_6 K_z), \tag{43c}$$
$$B_y(L_{3x}) = -R_3 q_x - R_4 K_x, \tag{43d}$$
$$A(L_{3y}) = i(\Xi_1 q_x + \Xi_2 K_x), \tag{43e}$$
$$B_z(L_{3y}) = R_1 q_y + R_2 K_y, \tag{43f}$$
$$B_x(L_{3y}) = -R_3 q_x - R_4 K_x, \tag{43g}$$
$$B_y(L_{3y}) = R_3 q_y + R_4 K_y + R_5 q_z + R_6 K_z, \tag{43h}$$

and

$$A(L_1) = -i(\Xi_3 q_z + \Xi_4 K_z), \tag{44a}$$
$$B_x(L_1) = R_7 q_y + R_8 K_y, \tag{44b}$$
$$B_y(L_1) = -(R_7 q_x + R_8 K_x), \tag{44c}$$

with $L_{3x} \sim -zy$ and $L_{3y} \sim zx$ being the basis functions of L_3 irreducible representation. For the $L_{2'}$ phonon, the second-order terms are nonvanishing in both the spin-conserving and spin-flip processes. Nevertheless, its contribution to the spin-conserving process is negligible compared to the zeroth-order contribution $A_{\mathbf{k}_\Gamma,\mathbf{k}_L}(L_{2'})$. As there is no zeroth-order term in the spin-flip process, the second-order spin-flip terms become important and read

$$B_z(L_{2'}) = iC_1(\mathbf{K} \times \mathbf{q})_z, \tag{45}$$

and

$$[B_x(L_{2'}), B_y(L_{2'})] = i\sum_{j=2}^{8} C_j(S_x^{(j)}, S_y^{(j)}), \tag{46}$$

with

$$(S_x^{(2)}, S_y^{(2)}) = K_z(K_y, -K_x), \tag{47a}$$
$$(S_x^{(3)}, S_y^{(3)}) = K_z(q_y, -q_x), \tag{47b}$$
$$(S_x^{(4)}, S_y^{(4)}) = q_z(q_y, -q_x), \tag{47c}$$
$$(S_x^{(5)}, S_y^{(5)}) = q_z(K_y, -K_x), \tag{47d}$$
$$(S_x^{(6)}, S_y^{(6)}) = (K_x^2 - K_y^2, -2K_xK_y), \tag{47e}$$
$$(S_x^{(7)}, S_y^{(7)}) = (q_x^2 - q_y^2, -2q_xq_y), \tag{47f}$$
$$(S_x^{(8)}, S_y^{(8)}) = (K_xq_x - K_yq_y, -K_xq_y - K_yq_x). \tag{47g}$$

The coefficients in Eqs. (43)-(47) are given in Table V and the spin-orientation dependence of the first- and second-order scattering matrices are expressed by Eq. (15). Note we have again omitted the subscripts $\mathbf{k}$ and $\mathbf{k}'$ in Eqs. (43)-(47). One can see that the first-order spin-conserving terms (Ξ_i) are much larger than the spin-flip ones (R_i). We also show the first-order contributions (of the L_3 and L_1 phonons) and second-order one (of the $L_{2'}$ phonon) to the spin-flip processes of the inter–Γ-L scattering in the spherical-band approximation in Table V for completeness.

2. *Inter–L-L valley scattering*

Recently, Tang *et al.*[15] and Li *et al.*[18] demonstrated the inter-L valley electron-phonon scattering with the X-point phonons (belong to X_3, X_1 and X_4 irreducible representations) involved.[2,29] Tang *et al.*[15] gave the general selection rules for the zeroth-order scattering matrix element and calculated the average values of both the zeroth- and first-order contributions, where the zeroth-order X_3-phonon contribution is forbidden. Li *et al.*[18] further derived the spin-orientation dependence and complete scattering matrices for the zeroth-order contributions, which were expressed with coefficients $D_{X_1,m}$, $D_{X_1,s}$ and $D_{X_4,s}$. Here $D_{X_1,m}$ corresponds to the spin-conserving process only and the $D_{X_1,s}$ and $D_{X_4,s}$ are coefficients for both the spin-flip and spin-conserving processes. In this work we additionally derive the explicit scattering matrix for the first-order terms of the X_3-phonon contribution with the method of invariants, which are shown to be non-negligible for the intrinsic electron spin relaxation in Ge in low temperature due to the relative low X_3-phonon energy.[18]

As the scatterings between the four L valleys are equivalent except for the coordinate rotations, we consider the $(\pi/a)(1,1,1) \leftrightarrow (\pi/a)(1,1,-1)$ case only and take the crystallographic frame for simplicity. The space symmetry of this scattering is described by one subgroup of the G_{32}^2 group (See Table VI),[2,15,18,34] where the 2-fold X_3 irreducible representation in G_{32}^2 group can be deduced into two one-dimensional (1D) representations and the wave-vectors and Pauli matrices belong to 1D representations also. Based on the space symmetry of the initial/final states, phonon states, wave-vectors and Pauli matrices (shown in Table VI) and the time-reversal symmetry, we construct the complete scattering matrix,

$$A(X_3^-) = -i\Xi_1(q_x - q_y), \tag{48a}$$

$$B_z(X_3^-) = R_1(K_x + K_y) + R_2 q_z, \tag{48b}$$

$$B_x(X_3^-) = R_3(q_x + q_y) + R_4(q_x - q_y) + R_5 K_z, \tag{48c}$$

$$B_y(X_3^-) = R_3(q_x + q_y) - R_4(q_x - q_y) + R_5 K_z. \tag{48d}$$

Here $X_3^\pm \sim (\sin\frac{4\pi x}{a} \pm \sin\frac{4\pi y}{a})(\cos\frac{2\pi z}{a} \pm \sin\frac{2\pi z}{a})$ are the basis functions of the X_3 irreducible representation and the X_3^+-phonon contribution is forbidden by the space symmetry (See Table VI). $\mathbf{K} = \mathbf{k}' - \mathbf{k}_{\rm i} + \mathbf{k} - \mathbf{k}_{\rm f}$ and $\mathbf{q} = \mathbf{k}' - \mathbf{k}_{\rm i} - (\mathbf{k} - \mathbf{k}_{\rm f})$ with $\mathbf{k}_{\rm i} = (\pi/a)(1,1,1)$ and $\mathbf{k}_{\rm f} = (\pi/a)(1,1,-1)$. The coefficients are given in Table VII and the spin-orientation dependence is given by Eq. (15). One can see that the X_3 phonons contribute to both the spin-conserving and spin-flip processes of the inter–L-L scattering, and the spin-conserving one is much larger (about 2 orders of magnitude) than the spin-flip one. We also calculate the spin-flip first-order contribution of the X_3 phonons in the spherical-band-approximation and the zeroth-order contributions of the X_1 and X_4 phonons for the sake of completeness (listed in Table VII), where we take the same notations for the zeroth-order scattering matrices as those in Li's work.[18] The parameters are in the same order with those in the previous works.[15,18]

TABLE VI: The space symmetry of the final/initial electron states, phonon states, wave-vectors and Pauli matrices in one subgroup of the G_{32}^2 group for the $(\pi/a)(1,1,1) \leftrightarrow (\pi/a)(1,1,-1)$ scattering.[2,18,34] Here $\tilde{\sigma}_\pm = \frac{1}{\sqrt{2}}(\sigma_x \pm \sigma_y)$, $\tilde{k}_\pm = \frac{1}{\sqrt{2}}(k_x \pm k_y)$ and $\tau = (a/4)(1,1,1)$. $X_3^\pm$ are the basis functions of the X_3 irreducible representations in the G_{32}^2 group, which are given in main text.

g	I	$\tilde{\sigma}_\pm$	σ_z	$\tilde{k}_\pm$	k_z	$X_3^\pm$	L_1	L_{1t}
$(E\|0)$	1	1	1	1	1	1	1	1
$(C_{2xy}\|\tau)$	1	±1	-1	±1	-1	1	$-L_{1t}$	L_1
$(C_{2x\bar{y}}\|\tau)$	1	∓1	-1	∓1	-1	-1	1	-1
$(C_{2z}\|0)$	1	-1	1	-1	1	-1	L_{1t}	L_1
$(i\|\tau)$	1	1	1	-1	-1	∓1	1	-1
$(\rho_{xy}\|0)$	1	±1	-1	∓1	1	∓1	L_{1t}	L_1
$(\rho_{x\bar{y}}\|0)$	1	∓1	-1	±1	1	±1	1	1
$(\rho_z\|\tau)$	1	-1	1	1	-1	±1	$-L_{1t}$	L_1

TABLE VII: The coefficients in the inter–L-L valley electron-phonon scattering matrix. In the first two columns, the Ξ_i and R_is stand for the parameters of the first-order scattering matrices of X_3 phonons and $D_1(X_3)$ is that for the first-order X_3-phonon spin-flip scattering element in the spherical-band-approximation with the spin eigenstates along the [001] direction. The last two columns show the coefficients of the zeroth-order contributions to the scattering matrix.[18]

	eV		eV/nm
Ξ_1	6.49	$D_{X_1,s}$	0.18
R_1	-3.65×10^{-2}	$D_{X_4,s}$	0.66
R_2	-1.43×10^{-1}	$D_{X_1,m}$	6.56
R_3	4.58×10^{-2}		
R_4	-5.17×10^{-2}		
R_5	8.68×10^{-2}		
$D_1(X_3)$	6.71×10^{-2}		

D. Elliott and Yafet mechanisms

In this part we analyze the Elliott[38] and Yafet[33] mechanisms in the spin-flip part of the electron-phonon scattering, where the electron-phonon interaction can be generally expressed as[32,33]

$$H_{\mathrm{ep}} = \sum_{\mathbf{q},\lambda} \mathbf{u}_{\mathbf{q},\lambda} \cdot \nabla [V_0(\mathbf{r})\hat{I} + \frac{\hbar}{4m_0^2c^2}(\nabla V_0(\mathbf{r}) \times \mathbf{p}) \cdot \boldsymbol{\sigma}]. \quad (49)$$

Here $\mathbf{u}_{\mathbf{q},\lambda}$ is the phonon displacement vector and $\mathbf{q}$ (λ) denotes the phonon wave vector (phonon mode). $V_0(\mathbf{r})\hat{I}$ represents the bare potential and $\frac{\hbar}{4m_0^2c^2}(\nabla V_0(\mathbf{r}) \times \mathbf{p}) \cdot \boldsymbol{\sigma}$ stands for the spin-orbit coupling. It should be noted that the bare potential and the spin-orbit coupling, which correspond to the Elliott and Yafet processes separately, share the same symmetry in all the point groups of the crystal. Therefore their scattering matrices have the same analytical forms with the total electron-phonon scattering matrices, which are the sum of the Elliott and Yafet ones.

For the spin-flip intravalley scattering, the wave-vector order analysis is clear in the centrosymmetric crystal.[18,33,38] Our analytical results are [See Eqs. (23), (31) and (32)] in agreement with the previous statements.[18,32,33,38] In the AC-phonon induced scattering, the first-order (K_l) contributions to the Elliott and Yafet processes cancel each other completely and the third-order terms ($K_l q_m q_n$) remain. While in the OP case, the leading-order terms of both the Elliott and Yafet mechanisms are second-order ($K_l q_m$) and there is no such perfect cancellation. Here $l, m, n \in \{x, y, z\}$. In our numerical calculation, the first-order contributions to the Elliott and Yafet processes in the AC spin-flip scattering are much larger (more than three orders of magnitude) than the total third-order spin-flip scattering matrix elements; and both the Elliott and Yafet terms in OP cases are in the same order with the total spin-flip matrix elements.

TABLE VIII: The coefficients for the zeroth-order contributions of the Elliott and Yafet mechanisms in the inter–Γ-L and inter-L valley electron-phonon scattering matrices. The superscript "E" ("Y") stands for the Elliott (Yafet) mechanism. The first two lines represent the parameters of the spin-flip inter–Γ-L scattering and the following four lines stand for those in the inter-L case. One can see that the coefficients in Tables V and VII are sums of the corresponding Elliott and Yafet ones in this table.

	eV/nm
$iB^{\mathrm{E}}_{\mathbf{k}_\Gamma,\mathbf{k}_L;y}(L_{3'})$	−0.10
$iB^{\mathrm{Y}}_{\mathbf{k}_\Gamma,\mathbf{k}_L;y}(L_{3'})$	0.45
$D^{\mathrm{E}}_{1,s}(X_1)$	−0.08
$D^{\mathrm{Y}}_{1,s}(X_1)$	0.26
$D^{\mathrm{E}}_{4,s}(X_4)$	0.25
$D^{\mathrm{Y}}_{4,s}(X_4)$	0.41

We then turn to the Elliott-Yafet mechanism in the zeroth-order spin-flip inter–Γ-L and inter-L valley scatterings, where our pseudo-potential calculation of the Elliott-Yafet coefficients are listed in Table VIII. Generally, the Elliott and Yafet contributions are in the same order with those of the total scattering matrices, which are simply sums of the corresponding Elliott-Yafet coefficients (See Tables V and VII). We further analyze the zeroth-order contribution of these two mechanisms with the Γ- and L-point $\boldsymbol{k} \cdot \boldsymbol{p}$ eigenstates [See Eqs. (33) and (12)], and give the explicit expressions with the single-group basis functions. For the inter–Γ-L valley scattering, the Elliott-Yafet matrix elements can be expressed as

$$\begin{aligned} iB^{\mathrm{E}}_{\mathbf{k}_\Gamma,\mathbf{k}_L;y}(L_{3'}) &= -\frac{c}{A}\langle \Gamma_2^- \uparrow | V^{\mathrm{E}}_{L_{3'(2)}} | L_{3(1)} \uparrow \rangle, && (50) \\ iB^{\mathrm{Y}}_{\mathbf{k}_\Gamma,\mathbf{k}_L;y}(L_{3'}) &= \frac{1}{A}[\langle \Gamma_2^- \uparrow | V^{\mathrm{Y}}_{L_{3'(2)}} | L_1 \downarrow \rangle \\ &\quad - c\langle \Gamma_2^- \uparrow | V^{\mathrm{Y}}_{L_{3'(2)}} | L_{3(1)} \uparrow \rangle], && (51) \end{aligned}$$

where ↑ (↓) is the spin eigenstate along the [111] direction and the superscript "E" ("Y") denotes the Elliott (Yafet) mechanism. One can see that the coupling between the lowest and upper conduction bands (L_1 and L_3) at the L-point is critical to the Elliott contribution, which is non-negligible in the total scattering matrix element. Here the Yafet contribution is about 4 times larger then the Elliott one (See Table VIII). For the inter-L valley scattering, we consider the scattering between $\mathbf{k}_{L_t} = \frac{\pi}{a}(1,1,-1)$ and $\mathbf{k}_L = \frac{\pi}{a}(1,1,1)$ and take the spin eigenstates along the [001] direction. The Elliott-Yafet matrix elements are given by

$$\begin{aligned} D^{\mathrm{E}}_{1,s}(X_1) &= -\frac{\sqrt{2}c}{2A^2}[\langle L_1^t \uparrow' | V^{\mathrm{E}}_{X_1} | (L_{3y} + i\cos\theta L_{3x}) \uparrow' \rangle \\ &\quad - \langle (L^t_{3y} + i\cos\theta L^t_{3x}) \downarrow' | V^{\mathrm{E}}_{X_1} | L_1 \downarrow' \rangle], && (52) \\ D^{\mathrm{Y}}_{1,s}(X_1) &= -\frac{\sqrt{2}c}{2A^2}[\langle L_1^t \uparrow' | V^{\mathrm{E}}_{X_1} | (L_{3y} + i\cos\theta L_{3x}) \uparrow' \rangle \\ &\quad - \langle (L^t_{3y} + i\cos\theta L^t_{3x}) \downarrow' | V^{\mathrm{E}}_{X_1} | L_1 \downarrow' \rangle] \\ &\quad - \frac{\sqrt{2}e^{i\phi}}{2A^2}[\langle L_1^t \uparrow' | V^{\mathrm{Y}}_{X_1} | L_1 \downarrow' \rangle \\ &\quad + ic\sin\theta(\langle L^t_{3x} \uparrow' | V^{\mathrm{Y}}_{X_1} | L_1 \downarrow' \rangle \\ &\quad + \langle L_1^t \uparrow' | V^{\mathrm{Y}}_{X_1} | L_{3x} \downarrow' \rangle)], && (53) \end{aligned}$$

and

$$D^{\rm E}_{1,s}(X_4) = -\frac{i}{A^2}[ic\sin\theta(\langle L^t_{3x}\uparrow'|V^{\rm E}_{X_4}|L_1\uparrow'\rangle - \langle L^t_1\uparrow'|V^{\rm E}_{X_4}|L_{3x}\uparrow'\rangle)], \tag{54}$$

$$\begin{aligned} D^{\rm Y}_{1,s}(X_4) = -\frac{i}{A^2}\{&[ic\sin\theta(\langle L^t_{3x}\uparrow'|V^{\rm Y}_{X_4}|L_1\uparrow'\rangle - \langle L^t_1\uparrow'|V^{\rm Y}_{X_4}|L_{3x}\uparrow'\rangle)] \\ &- c[e^{i\phi}\langle L^t_1\uparrow'|V^{\rm Y}_{X_4}|(L_{3y}-i\cos\theta L_{3x})\downarrow'\rangle \\ &+ e^{-i\phi}\langle(L^t_{3y}+i\cos\theta L^t_{3x})\downarrow'|V^{\rm Y}_{X_4}|L_1\uparrow'\rangle]\}, \end{aligned} \tag{55}$$

where the superscript "t" stands for the wave function at the $\mathbf{k}_{L_t}$ point and $\uparrow'$ ($\downarrow'$) is the spin eigenstate along the [001] direction. $\theta = \arccos\frac{\sqrt{3}}{3}$ and $\phi = \frac{\pi}{4}$. We omit the c^2 terms in Eqs. (55)-(53) as $c \sim 10^{-2}$. Here the mixing between the lowest and higher conduction bands leads to the Elliott process in $D_{1,s}(X_1)$ and both the Elliot and Yafet ones in $D_{1,s}(X_4)$. The Elliott and Yafet contributions are comparable also in this case (See Table VIII). The scatterings between other L points are similar to this case and we ignore the discussions in this work.

IV. SUMMARY

In summary, we have investigated the electron-phonon scatterings of the L and Γ valleys, and studied the energy spectra near the bottom of the conduction bands with the L-point $\boldsymbol{k}\cdot\boldsymbol{p}$ Hamiltonian in Ge. We first construct a 16×16 $\boldsymbol{k}\cdot\boldsymbol{p}$ Hamiltonian in the vicinity of the L point with the double-group basis functions, of which the energy spectra of the lowest three conduction and highest two valence bands agree with the tight-binding model ones. The eigenstates of this Hamiltonian are useful for the analysis of the spin-related properties in Ge.

We then study the phonon-induced electron scatterings of the L and Γ valleys in Ge, i.e., the intra-Γ/L valley, inter–Γ-L valley and inter-L valley scatterings. Via the symmetry consideration, we derive the selection rules and compact scattering matrices in all these cases, among which the scattering matrices for the intra-Γ valley, inter–Γ-L valley, OP contribution and the separated TA and LA contributions of the intra-L valley scatterings are absent in the literature. We show the lowest-order wave-vector dependence of the scattering matrices for all the related phonon modes, where the zeroth-order spin-flip scattering matrix elements are absent (present) in the intra- (inter-) valley cases. For completeness we also give the lowest non-zeroth order contributions in the inter-valley cases in the spherical band approximation. The spin-orientation dependence of the electron-phonon scattering can be easily obtained with the corresponding scattering matrix. Our pseudo-potential calculation provides the coefficients of these scattering matrices, and confirms the selection rules and wave-vector dependence. Finally, we analyze the Elliott and Yafet mechanisms in these electron-phonon scatterings with the $\boldsymbol{k}\cdot\boldsymbol{p}$ eigenstates at the L and Γ valleys. This investigation provides the necessary electron-phonon scatterings for the study of the optical orientation of spin and the hot-electron relaxation in Ge.

Acknowledgments

This work was supported by the National Basic Research Program of China under Grant No. 2012CB922002 and the Strategic Priority Research Program of the Chinese Academy of Sciences under Grant No. XDB01000000.

Appendix A: THE $\boldsymbol{k}\cdot\boldsymbol{p}$ BASIS FUNCTIONS

TABLE IX: The basis functions representing 16 L-point Bloch states, 4 in the valence band and 12 in the conduction band.

Band state	Basic functions	$H_{0,jj}$
$\lvert v1\rangle = L_4^-(L_{3'}^v)$	$\frac{1}{2}[(x-{\rm i}y)\downarrow -(x+{\rm i}y)\uparrow]$	E^-_{45v}
$\lvert v2\rangle = L_5^-(L_{3'}^v)$	$\frac{1}{2}[(x-{\rm i}y)\downarrow +(x+{\rm i}y)\uparrow]$	E^-_{45v}
$\lvert v3\rangle = L_{6(1)}^-(L_{3'}^v)$	$\frac{1}{\sqrt{2}}(x+iy)\downarrow= L_{3'(2)}\downarrow$	E^-_{6v}
$\lvert v4\rangle = L_{6(2)}^-(L_{3'}^v)$	$-\frac{1}{\sqrt{2}}(x-iy)\uparrow= -L_{3'(1)}\uparrow$	E^-_{6v}
$\lvert c1\rangle = L_{6(1)}^+(L_1)$	$s\uparrow$	E^+_{6c}
$\lvert c2\rangle = L_{6(2)}^+(L_1)$	$s\downarrow$	E^+_{6c}
$\lvert c3\rangle = L_{6(2)}^+(L_3)$	$z(x-iy)\uparrow$; $i(x+iy)^2\uparrow$	$E^+_{6c'}$
$\lvert c4\rangle = L_{6(1)}^+(L_3)$	$-z(x+iy)\downarrow$; $i(x-iy)^2\downarrow$	$E^+_{6c'}$
$\lvert c5\rangle = L_4^+(L_3)$	$\frac{1}{\sqrt{2}}z[(x-{\rm i}y)\downarrow +(x+{\rm i}y)\uparrow]$; $\frac{i}{\sqrt{2}}[-(x-iy)^2\uparrow +(x+iy)^2\downarrow]$	E^+_{45c}
$\lvert c6\rangle = L_5^+(L_3)$	$\frac{1}{\sqrt{2}}z[(x-{\rm i}y)\downarrow -(x+{\rm i}y)\uparrow]$; $\frac{i}{\sqrt{2}}[(x-iy)^2\uparrow +(x+iy)^2\downarrow]$	E^+_{45c}
$\lvert c7\rangle = L_4^-(L_{3'}^c)$	the same as $L_4^-(L_{3'}^v)$	E^-_{45c}
$\lvert c8\rangle = L_5^-(L_{3'}^c)$	see $L_5^-(L_{3'}^v)$	E^-_{45c}
$\lvert c9\rangle = L_{6(1)}^-(L_{3'}^c)$	see $L_{6(1)}^-(L_{3'}^v)$	E^-_{6c}
$\lvert c10\rangle = L_{6(2)}^-(L_{3'}^c)$	see $L_{6(2)}^-(L_{3'}^v)$	E^-_{6c}
$\lvert c11\rangle = L_{6(1)}^-(L_{2'})$	$z\uparrow$	$E^-_{6c'}$
$\lvert c12\rangle = L_{6(2)}^-(L_{2'})$	$z\downarrow$	$E^-_{6c'}$

In Table IX, in order to define the transformation matrices for the 16 L-point Bloch functions used in our $\boldsymbol{k}\cdot\boldsymbol{p}$ Hamiltonian, we explicitly give in the second column simple examples of the corresponding basis functions. The first column presents the state notation $|v,j\rangle$ with $j = 1\ldots4$ or $|c,j\rangle$ ($j = 1\ldots12$), the double-group representation and, in brackets, the corresponding single-group representation. For example, the symbol $L^-_{6(2)}(L^v_{3'})$ means the second state of the representation L^-_6 originating from the valence-band representation $L_{3'}$. The arrow $\uparrow$ ($\downarrow$) symbolizes the spin-up (down) eigenstate along the $\hat{z}$ direction. For each of the representations L_4^+, L_5^+ we give two different examples of the basis functions. The notation of the diagonal energies $H_{0,jj}$ is shown in the third column. Finally, in construction of the basis functions, we set one of the planes σ_v contain the axes y and z in the D_{3d} group.

---

[*] Electronic address: `ivchenko@coherent.ioffe.ru`

[†] Electronic address: `mwwu@.ustc.edu.cn.`

[1] I. Žutić, J. Fabian, and S. Das Sarma, Rev. Mod. Phys. **76**, 323 (2004).

[2] P. Y. Yu and M. Cardona, *Fundamentals of Semiconductors: Physics and Materials Properties* (Springer, New York, 2001), 3rd ed.

[3] D. Culcer, L. Cywiński, Q. Li, X. Hu, and S. Das Sarma, Phys. Rev. B **80**, 205302 (2009).

[4] N. W. Gray and A. Tiwari, Appl. Phys. Lett. **98**, 102112 (2011).

[5] K. R. Jeon, B. C. Min, I. J. Shin, C. Y. Park, H. S. Lee, Y. H. Jo, and S. C. Shin, Appl. Phys. Lett. **98**, 262102 (2011).

[6] B. T. Jonker, G. Kioseoglou, A. T. Hanbicki, C. H. Li, and P. E. Thompson, Nat. Phys. **3**, 542 (2007).

[7] I. Appelbaum, B. Huang, and D. J. Monsma, Nature **447**, 295 (2007).

[8] L. Grenet, M. Jamet, P. Noé, V. Calvo, J. M. Hartmann, L. E. Nistor, B. Rodmacq, S. Auffret, P. Warin, and Y. Samson, Appl. Phys. Lett. **94**, 032502 (2009).

[9] S. P. Dash, S. Sharma, R. S. Patel, M. P. de Jong, and R. Jansen, Nature **462**, 491 (2009).

[10] E. J. Loren, B. A. Ruzicka, L. K. Werake, H. Zhao, H. M. van Driel, and A. L. Smirl, Appl. Phys. Lett. **95**, 092107 (2009).

[11] J. Rioux and J. E. Sipe, Phys. Rev. B **81**, 155215 (2010).

[12] E. J. Loren, J. Rioux, C. Lange, J. E. Sipe, H. M. van Driel, and A. L. Smirl, Phys. Rev. B **84**, 214307 (2011).

[13] P. Li and H. Dery, Phys. Rev. Lett. **107**, 107203 (2011).

[14] A. Jain, L. Louahadj, J. Peiro, J. C. Le Breton, C. Vergnaud, A. Barski, C. Beigné, L. Notin, A. Marty, V. Baltz, S. Auffret, E. Augendre, H. Jaffrès, J. M. George, and M. Jamet, Appl. Phys. Lett. **99**, 162102 (2011).

[15] J. M. Tang, B. T. Collins, and M. E. Flatté, Phys. Rev. B **85**, 045202 (2012).

[16] F. Pezzoli, F. Bottegoni, D. Trivedi, F. Ciccacci, A. Giorgioni, P. Li, S. Cecchi, E. Grilli, Y. Song, M. Guzzi, H. Dery, and G. Isella, Phys. Rev. Lett. **108**, 156603 (2012).

[17] A. Jain, C. Vergnaud, J. Peiro, J. C. Le Breton, E. Prestat, L. Louahadj, C. Portemont, C. Ducruet, V. Baltz, A. Marty, A. Barski, P. Bayle-Guillemand, L. Vila, J. P. Attané, E. Augendre, H. Jaffrès, J. M. George, and M. Jamet, Appl. Phys. Lett. **101**, 022402 (2012).

[18] P. Li, Y. Song, and H. Dery, Phys. Rev. B **86** 085202 (2012).

[19] P. Li, D. Trivedi, and H. Dery, arXiv:1211.7292.

[20] Y. Zhou, W. Han, L. T. Chang, F. Xiu, M. Wang, M. Oehme, I. A. Fischer, J. Schulze, R. K. Kawakami, and K. L. Wang, Phys. Rev. B **84**, 125323 (2011).

[21] C. Tahan, M. Friesen, and R. Joynt, Phys. Rev. B **66**, 035314 (2002).

[22] M. S. Sherwin, A. Imamoglu, and T. Montroy, Phys. Rev. A **60**, 3508 (1999).

[23] A. R. Calderbank and P. W. Shor, Phys. Rev. A **54**, 1098 (1996).

[24] C. H. Bennett, D. P. DiVincenzo, J. A. Smolin, and W. K. Wootters, Phys. Rev. A **54**, 3824 (1996).

[25] D. G. Cory, M. D. Price, W. Maas, E. Knill, R. Laflamme, W. H. Zurek, T. F. Havel, and S. S. Somaroo, Phys. Rev. Lett. **81**, 2152 (1998).

[26] A. R. Cameron, P. Riblet, and A. Miller, Phys. Rev. Lett. **76**, 4793 (1996).

[27] J.-M. Jancu, R. Scholz, F. Beltram, and F. Bassani, Phys. Rev. B **57**, 6493 (1998).

[28] Y. H. Kuo, Y. K. Lee, Y. Ge, S. Ren, J. E. Roth, T. I. Kamins, D. A. B. Miller, and J. S. Harris, Nature **437**, 1334 (2005).

[29] M. S. Dresselhaus, G. Dresselhaus, and A. Jorio, *Group Theory: Application to the Physics of Condensed Matter* (Springer, Berlin, 2008).

[30] L. C. L. Y. Voon and M. Willatzen, *The $\boldsymbol{k} \cdot \boldsymbol{q}$ Method: Electronic Properties of Semiconductors* (Springer, Berlin, 2009).

[31] G. L. Bir and G. E. Pikus, *Symmetry and Strain-Induced Effects in Semiconductors*, (Halsted, Jerusalem, 1974).

[32] Y. Song and H. Dery, Phys. Rev. B **86**, 085201 (2012).

[33] Y. Yafet, in *Solid State Physics*, edited by F. Seitz and D. Turnbull (Academic, New York, 1963), Vol. 14, p. 1.

[34] M. Lax and J. J. Hopfield, Phys. Rev. **124**, 115 (1961).

[35] M. Lax, Phys. Rev. **138**, A793 (1965).

[36] E. McCann and V. I. Fal'ko, Phys. Rev. Lett. **108**, 166606 (2012).

[37] H. Ochoa, A. H. C. Neto, V. I. Fal'ko, and F. Guinea, arXiv:1209.4382.

[38] R. J. Elliott, Phys. Rev. **96**, 266 (1954).

[39] S. Ridene, K. Boujdaria, H. Bouchriha, and G. Fishman, Phys, Rev. B **64**, 085329 (2001).

[40] R. Winkler, *Spin-obit coupling effects in two-dimensional electron and hole systems* (Springer, Berlin, 2003).

[41] V.D. Dymnikov, Phys. Solid State **43**, 2037 (2001).

[42] J. Rioux and J. E. Sipe, Physica E **45**, 1 (2012).

[43] P. Zhang, J. Zhou, and M. W. Wu, Phys. Rev. B **77**, 235323 (2008).

[44] D. K. Ferry, Phys. Rev. B **14**, 1605 (1976).

[45] J. L. Cheng, J. Rioux, J. Fabian, and J. E. Sipe, Phys. Rev. B **83**, 165211 (2011).

[46] J. L. Cheng, M. W. Wu, and J. Fabian, Phys. Rev. Lett. **104**, 016601 (2010).

[47] P. Li and H. Dery, Phys. Rev. Lett. **105**, 037204 (2010).

[48] M. M. Rieger and P. Vogl, Phys. Rev. B **48**, 14276 (1993).

[49] W. Weber, Phys. Rev. B **15**, 4789 (1977).